Self-Motions of General 3-*RPR* Planar Parallel Robots

Sébastien Briot
Vigen Arakelian
Département de Génie Mécanique et Automatique,
Institut National des Sciences Appliquées (INSA), Rennes, France
sebastien.briot@ens.insa-rennes.fr

Ilian A. Bonev
Department of Automated Production Engineering,
École de Technologie Supérieure (ÉTS), Montréal, Canada

Damien Chablat
Philippe Wenger
Institut de Recherche en Communications et Cybernétique de Nantes
1, rue la Noë – BP 92101 44321, Nantes Cedex 3, France

Abstract

We study the kinematic geometry of general 3-RPR planar parallel robots with actuated base joints. These robots, while largely overlooked, have simple direct kinematics and large singularity-free workspace. Furthermore, their kinematic geometry is the same as that of a newly developed parallel robot with SCARA-type motions. Starting from the direct and inverse kinematic model, the expressions for the singularity loci of 3-RPR planar parallel robots are determined. Then, the global behavior at all singularities is geometrically described by studying the degeneracy of the direct kinematic model. Special cases of self-motions are then examined and the degree of freedom gained in such special configurations is kinematically interpreted. Finally, a practical example is discussed and experimental validations performed on an actual robot prototype are presented.

KEY WORDS—planar parallel robot, kinematic geometry, singularity, self-motion

1. Introduction

From an industrial point of view, the complexity and existence of numerous singular configurations seems to be the worst drawback of parallel robots as these configurations reduce the size of the workspace, which is already smaller than that of similarly-sized serial robots. Fortunately, the determination of singularities is a well-researched problem and several computational methods have already been presented (Gosselin and Angeles 1990; Zlatanov et al. 1994; Bonev et al. 2003).

The International Journal of Robotics Research
Vol. 27, No. 7, July 2008, pp. 855–866
DOI: 10.1177/0278364908092466

The worst singular configuration a parallel robot can meet is the Type 2 singularity (Gosselin 1990). In such a singularity, the robot gains at least one degree of freedom and cannot resist some wrenches applied to its platform. Furthermore, the robot cannot exit such a singular configuration without external help. Type 2 singular configurations can be divided into two classes depending on the nature of the degree(s) of freedom gained, being either infinitesimal or finite, i.e. *self-motion*. However, by merely studying the Jacobian (Gosselin and Angeles 1990; Bonev et al. 2003), one cannot identify the nature of Type 2 singularities.

Symmetry and, more precisely, design conditions that simplify the generally too complex direct kinematics of parallel robots are often privileged by robot designers. Unfortunately, such design conditions usually lead to self-motions, which are certainly the worst type of singularity. Furthermore, as we show in this paper, self-motions also occur in unsymmetrical seemingly general designs without simplified direct kinematic models. Hence, it is essential that the design conditions for such self-motions be well known in order to be avoided.

Several papers discuss self-motions in parallel robots. Not surprisingly, most of them deal with the Gough-Stewart platform whose direct kinematic model leads to as many as 40 real solutions for a relatively general design. Design conditions simplifying the direct kinematics of Gough-Stewart platforms, subsequently leading to self-motions, are given in: Husty and Zsombor-Murray (1994); Karger and Husty (1998); Husty and Karger (2000); Karger (2001, 2003); Wohlhart (2003). A classification of all self-motions of the Stewart-Gough platform is presented in Karger and Husty (1998). It is shown that the self-motions can be translations, pure rotations, generalized screw motions, motions equivalent to the displacements

of spherical four-bar mechanisms or more complex spatial motions.

The Stewart-Gough platform is not the only parallel robot with self-motions. A few other parallel robots having self-motions have also been studied. For example, in Bonev et al. (2006), it is shown that all singularities of the special 3-*RRR* (*R* stands for a passive revolute joint, and *R* for an actuated revolute joint) spherical parallel robot, known as the Agile Eye, are self-motions. The analysis of self mobility of spatial 5*R* closed-loop mechanisms with one degree of freedom are presented in Karger (1998). Bandyopadhyay and Ghosal (2004) discuss the determination of generalized analytical expressions for the analysis of self-motions and present several examples for both planar and spatial mechanisms with legs composed of *R* joints.

In this paper, we study the self-motions of general 3-*RPR* planar parallel robots (*P* stands for a passive prismatic joint). The 3-*RPR* planar parallel robot has a simple direct kinematic model and, when properly designed, a relatively large singularity-free workspace. However, despite these advantages, only a couple of works deal with this kind of robot (Hayes 1999; Hayes and Zsombor-Murray 2004). However, a recently developed new decoupled parallel robot with SCARA-type motions (Briot and Arakelian 2007) has its planar displacements governed by the same kinematic model as that of a 3-*RPR* planar parallel robot. Furthermore, the self-motions of a particular design of a 3*RPR* planar parallel robot with congruent equilateral base and platform were studied in Chablat et al. (2006), mainly from a theoretical point of view. This paper basically generalizes that study and demonstrates the advantages of general 3-*RPR* planar parallel robots.

The rest of this paper is organized as follows. Section 2 deals with the kinematics of the general 3-*RPR* planar parallel robot. The direct and inverse kinematic models are derived from the closure equations, and the singularity analysis based on the observation of the rank of the Jacobian matrix is presented. Section 3 presents a self-motion analysis based on the degeneracy of the direct kinematic model. Singularity loci are given and the degree of freedom gained is kinematically interpreted. Section 4 deals with a particular case of 3-*RPR* planar parallel robot with equilateral base and platform triangles and the results obtained are validated on an actual robot prototype. Conclusions are drawn in Section 5.

2. Kinematics and Singularity Analysis

The following analysis is based on the schematics of the robot shown in Figure 1. The revolute joints A_i ($i = 1, 2, 3$) are fixed on the base and are actuated. Each leg is composed of one passive prismatic joint, placed between points A_i and B_i, and one passive revolute joint C_i, connected to the mobile platform.

We consider that we control the position (x, y) of point P from the mobile platform and the orientation ϕ of the mobile platform. The origin of the base frame is chosen at point

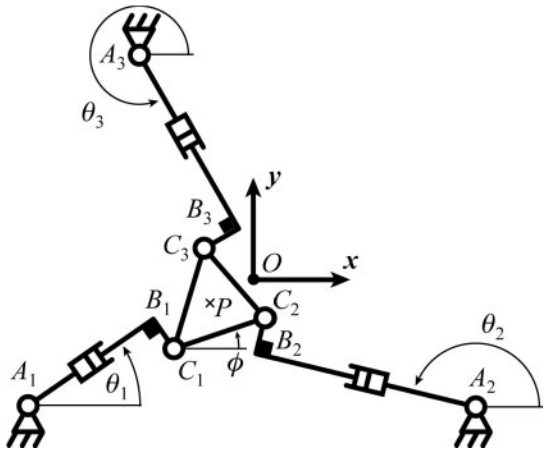

Fig. 1. Schematic representation of the 3-*RPR* planar parallel robot under study.

O. Points O and P are located at the centers of the circumscribed circles of triangles $A_1A_2A_3$ and $C_1C_2C_3$, respectively (Figure 2). Finally, let $\rho_i = |A_iB_i|$ and $L_i = |B_iC_i|$, the latter referred to as an *offset*.

It is therefore possible to express the position of points A_i and C_i as

$$\mathbf{OA}_i = \begin{bmatrix} x_{A_i} \\ y_{A_i} \end{bmatrix} = R_b \begin{bmatrix} \cos\gamma_i \\ \sin\gamma_i \end{bmatrix},$$

$$\mathbf{OC}_i = \begin{bmatrix} x_{C_i} \\ y_{C_i} \end{bmatrix} = \begin{bmatrix} x \\ y \end{bmatrix} + R_p \begin{bmatrix} \cos(\phi + \delta_i) \\ \sin(\phi + \delta_i) \end{bmatrix} \quad (1)$$

where $\gamma_i = (\alpha_b + \pi, -\alpha_b, -\alpha_b + \beta_b)$ and $\delta_i = (\alpha_p + \pi, -\alpha_p, -\alpha_p + \beta_p)$. From these expressions and referring to Bonev et al. (2003), one can determine the closure equations of the system:

$$\mathbf{OC}_i - \mathbf{OB}_i = \begin{bmatrix} x_{C_i} - x_{A_i} - \rho_i\cos\theta_i \\ y_{C_i} - y_{A_i} - \rho_i\sin\theta_i \end{bmatrix} = L_i \begin{bmatrix} -\sin\theta_i \\ \cos\theta_i \end{bmatrix}. \quad (2)$$

Refer to Bonev et al. (2003) for the full derivation. The velocity equation for the 3-*RPR* robot is:

$$\mathbf{A}\left[\dot{\phi}, \dot{x}, \dot{y}\right]^T = \mathbf{B}\left[\dot{\theta}_1, \dot{\theta}_2, \dot{\theta}_3\right]^T \quad (3)$$

with

$$\mathbf{A} = \begin{bmatrix} \mathbf{f}_1^T\mathbf{E}\mathbf{g}_1 & \mathbf{f}_1^T \\ \mathbf{f}_2^T\mathbf{E}\mathbf{g}_2 & \mathbf{f}_2^T \\ \mathbf{f}_3^T\mathbf{E}\mathbf{g}_3 & \mathbf{f}_3^T \end{bmatrix}, \quad \mathbf{B} = \begin{bmatrix} \rho_1 & 0 & 0 \\ 0 & \rho_2 & 0 \\ 0 & 0 & \rho_3 \end{bmatrix}, \quad (4)$$

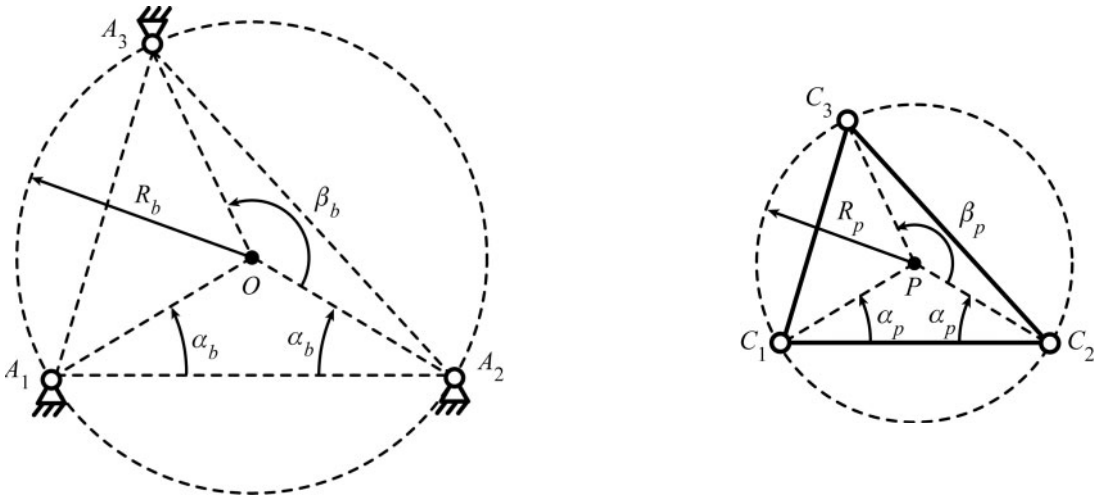

Fig. 2. Parameterization of the base and platform triangles: (a) fixed base and (b) mobile platform.

and

$$\mathbf{g}_i = \begin{bmatrix} x_{C_i} - x & y_{C_i} - y \end{bmatrix}^T, \quad \mathbf{E} = \begin{bmatrix} 0 & 1 \\ -1 & 0 \end{bmatrix},$$

$$\mathbf{f}_i = \begin{bmatrix} -\sin\theta_i \\ \cos\theta_i \end{bmatrix}. \tag{5}$$

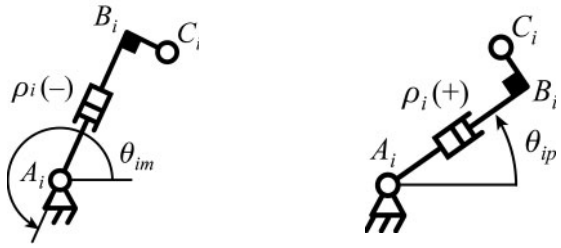

Fig. 3. The two inverse kinematic solutions of the *i*th leg of the robot: (a) first solution, ρ_i (+) and (b) second solution, ρ_i (–).

2.1. Inverse kinematic problem

Solving the inverse kinematics for each leg of this robot is essentially finding the intersection points between two circles, one with diameter $|A_iC_i|$ centered at the middle of segment A_iC_i, and one with radius L_i centered at C_i. Pre-multiplying both sides of Equation (2) with the term $\mathbf{f}_i^T$, one can obtain an equation expressing the angles θ_i as a function of the other parameters:

$$(x_{C_i} - x_{A_i})\sin\theta_i - (y_{C_i} - y_{A_i})\cos\theta_i - L_i = 0. \tag{6}$$

From Equation (6), it is possible to find the expressions for the active-joint variables θ_i as functions of the position (x, y) and the orientation ϕ of the mobile platform:

$$\theta_{ip} = 2\tan^{-1}\left(\frac{-(x_{Ci}-x_{Ai})+\sqrt{(x_{Ci}-x_{Ai})^2+(y_{Ci}-y_{Ai})^2-L_i^2}}{-L_i+y_{Ci}-y_{Ai}}\right), \tag{7a}$$

$$\theta_{im} = 2\tan^{-1}\left(\frac{-(x_{Ci}-x_{Ai})-\sqrt{(x_{Ci}-x_{Ai})^2+(y_{Ci}-y_{Ai})^2-L_i^2}}{-L_i+y_{Ci}-y_{Ai}}\right). \tag{7b}$$

The two solutions θ_{ip} and θ_{im} define the two inverse kinematic solutions for leg i (Figure 3). These define a total of eight solutions to the inverse kinematics of the parallel robot, also called *working modes* (Wenger and Chablat 1998). We will see that for this robot, provided there are non-zero offsets $L_i > 0$, the singularity loci will depend on the working mode.

2.2. Type 1 Singularities

Type 1 singularities occur when the determinant of **B** vanishes, i.e. when $\rho_i = 0$ (for i = 1, 2, or 3) (Figure 4) (Bonev et al. 2003). These configurations correspond to the internal boundaries of the workspace of a general 3-*RPR* planar parallel robot. When the offsets are zero, i.e. $L_i = 0$, there is a generic Type 1 (RI) singularity where the input velocities are indeterminate (Zlatanov et al. 1994). On this singularity, the inverse kinematic model of leg i admits only one solution because $(x_{Ci} - x_{Ai})^2 + (y_{Ci} - y_{Ai})^2 - L_i^2 = \rho_i^2 = 0$.

2.3. Direct Kinematic Problem

It is shown in Merlet (1996) that the solution of the direct kinematics of a 3*RPR* planar parallel robot is equivalent to finding

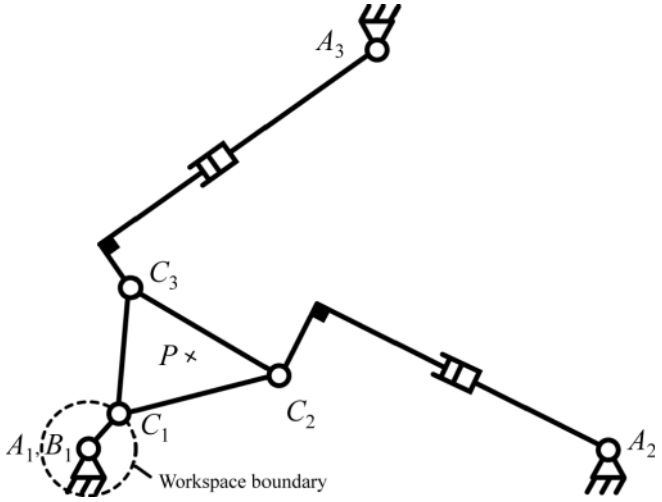

Fig. 4. Type 1 singularity.

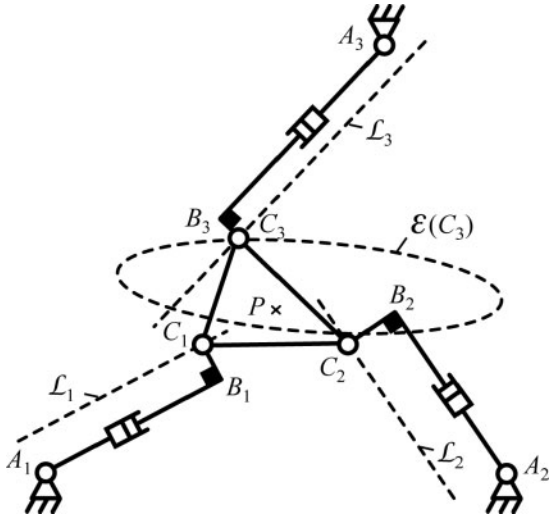

Fig. 5. Geometric interpretation of the direct kinematics.

the intersection points between an ellipse and a line, but no analytical expressions are given. Let us dismount the revolute joint at C_3. For given active-joint variables θ_1 and θ_2, points C_1 and C_2 are constrained to move along two lines, $\mathcal{L}_1$ and $\mathcal{L}_2$, respectively, and the mobile platform undergoes a Cardanic motion (Sekulie 1998; Tischler et al. 1998) (Figure 5). As a result, any points Q from the mobile platform, including P and C_i, describe a curve $\mathcal{E}(Q)$, which can be an ellipse, two parallel lines or a doubly-traced line segment. Thus, the direct kinematics can be solved by finding the intersection points between the curve $\mathcal{E}(C_3)$ and the line $\mathcal{L}_3$.

Let us now derive the expression of the elliptic curve $\mathcal{E}(C_3)$. It is possible to write the following closure equation:

$$\mathbf{OC}_3 = \mathbf{OA}_1 + \mathbf{A}_1\mathbf{B}_1 + \mathbf{B}_1\mathbf{C}_1 + \mathbf{C}_1\mathbf{C}_3. \tag{8}$$

This yields the expression:

$$\mathbf{OC}_3 = \begin{bmatrix} x_{C3} \\ y_{C3} \end{bmatrix} = \begin{bmatrix} x_{A1} \\ y_{A1} \end{bmatrix} + \rho_1 \begin{bmatrix} \cos\theta_1 \\ \sin\theta_1 \end{bmatrix} + L_1 \begin{bmatrix} -\sin\theta_1 \\ \cos\theta_1 \end{bmatrix} + 2R_p \cos\left(\frac{\beta_p}{2} - \alpha_p\right) \begin{bmatrix} \cos\left(\frac{\beta_p}{2} + \phi\right) \\ \sin\left(\frac{\beta_p}{2} + \phi\right) \end{bmatrix}. \tag{9}$$

In this expression, all parameters are known except ρ_1 and ϕ. However, they are dependent on each other. Without loss of generality, we choose ϕ as the independent variable and express ρ_1 as a function of ϕ, using the closure equation:

$$\mathbf{A}_1\mathbf{A}_2 = \mathbf{A}_1\mathbf{B}_1 + \mathbf{B}_1\mathbf{C}_1 + \mathbf{C}_1\mathbf{C}_2 + \mathbf{C}_2\mathbf{B}_2 + \mathbf{B}_2\mathbf{A}_2. \tag{10}$$

Developing this relation, we obtain:

$$\begin{bmatrix} x_{A2} - x_{A1} \\ y_{A2} - y_{A1} \end{bmatrix} = \rho_1 \begin{bmatrix} \cos\theta_1 \\ \sin\theta_1 \end{bmatrix} + L_1 \begin{bmatrix} -\sin\theta_1 \\ \cos\theta_1 \end{bmatrix} + 2R_p \cos\alpha_p \begin{bmatrix} \cos\phi \\ \sin\phi \end{bmatrix} - L_2 \begin{bmatrix} -\sin\theta_2 \\ \cos\theta_2 \end{bmatrix} - \rho_2 \begin{bmatrix} \cos\theta_2 \\ \sin\theta_2 \end{bmatrix}. \tag{11}$$

Expressing ρ_1 and ρ_2 as a function of ϕ from Equation (11), we obtain:

$$\rho_j = a_{j1} + a_{j2}\cos\phi + a_{j3}\sin\phi, \quad (j = 1, 2) \tag{12}$$

where the expressions for a_{ji} are given in the appendix. Substituting Equation (12) into Equation (9), we find the relation:

$$\mathbf{OC}_3 = \begin{bmatrix} x_{C3} \\ y_{C3} \end{bmatrix} = \begin{bmatrix} b_{11} + b_{12}\cos\phi + b_{13}\sin\phi \\ b_{21} + b_{22}\cos\phi + b_{23}\sin\phi \end{bmatrix}, \tag{13}$$

where b_{ji} $(j = 1, 2)$ are given in the appendix.

Therefore, for any fixed input parameters θ_i, we have found in Equation (13) the parametric expression of the elliptic curve $\mathcal{E}(C_3)$ depending on the orientation ϕ of the platform. Furthermore, we know that point C_3 belongs to line $\mathcal{L}_3$ with expression:

$$y = \tan\theta_3(x + L_3\sin\theta_3 - x_{A3}) + y_{A3} + L_3\cos\theta_3. \tag{14}$$

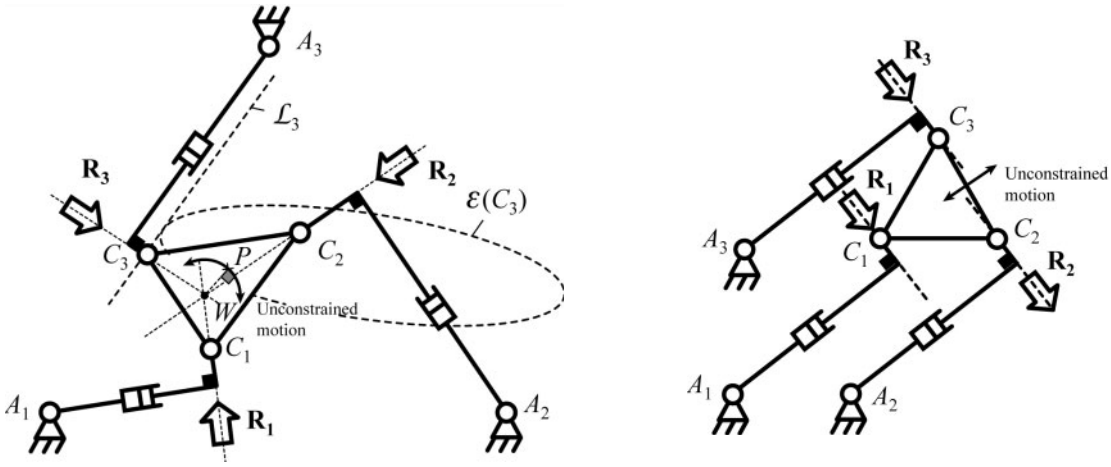

Fig. 6. Type 2 singularities of the parallel robot: (a) infinitesimal rotation about W and (b) finite translation (self-motion) along the direction of the prismatic joints.

Thus, the intersections between $\mathcal{E}(C_3)$ and $\mathcal{L}_3$ can be found by substituting x and y in Equation (14) by the expressions of x_{C3} and y_{C3} of Equation (13). After the substitution into Equation (14) and multiplying the equation by $\cos\theta_3$, we obtain:

$$\begin{aligned} 0 &= \sin\theta_3(x_{C3} + L_3\sin\theta_3 - x_{A3}) \\ &+ \cos\theta_3(y_{A3} + L_3\cos\theta_3 - y_{C3}). \end{aligned} \tag{15}$$

Developing Equation (15),

$$c_1 + c_2\cos\phi + c_3\sin\phi = 0, \tag{16}$$

where c_i are given in the appendix. From Equation (16), it is therefore possible to find the solution for ϕ:

$$\phi = 2\tan^{-1}\left(\frac{-c_3 \pm \sqrt{c_3^2 - c_1^2 + c_2^2}}{c_1 - c_2}\right). \tag{17}$$

Note that this solution is not unique and corresponds to the two assembly modes of the robot. Finally, it is possible to find the expression for the position using the closure equation:

$$\mathbf{OP} = \mathbf{OA}_1 + \mathbf{A}_1\mathbf{B}_1 + \mathbf{B}_1\mathbf{C}_1 + \mathbf{C}_1\mathbf{P} \tag{18}$$

which yields:

$$\begin{aligned} \mathbf{OP} &= \begin{bmatrix} x \\ y \end{bmatrix} = \begin{bmatrix} x_{A1} \\ y_{A1} \end{bmatrix} + \rho_1 \begin{bmatrix} \cos\theta_1 \\ \sin\theta_1 \end{bmatrix} \\ &+ L_1 \begin{bmatrix} -\sin\theta_1 \\ \cos\theta_1 \end{bmatrix} + R_p \begin{bmatrix} \cos(\phi + \alpha_p) \\ \sin(\phi + \alpha_p) \end{bmatrix}. \end{aligned} \tag{19}$$

2.4. Type 2 Singularities Analysis

Type 2 singularities occur when the determinant of **A** vanishes. It can be shown that the numerator of the determinant of matrix **A** contains three radicals and is dependent on the working mode. If we manipulate this expression properly and raise it to square three times, we can obtain a polynomial of degree 16 in x and y (Bonev et al. 2003). This polynomial will cover all working modes. Note, however, that if $L_i = 0$, the numerator becomes a quadratic polynomial in x and y and that the denominator of this expression is equal to $\rho_1\rho_2\rho_3$. Unfortunately, the study of this determinant cannot characterize the motion gained by the mobile platform at Type 2 singularities.

In a Type 2 singularity, the lines normal to the directions of the prismatic joints passing through points C_i are concurrent or parallel (Figure 6) (Bonev et al. 2003). These lines coincide with the direction of the forces $\mathbf{R}_i$ applied to the platform by the actuators.

However, we need more information for characterizing the complete kinematic behavior of the robot inside such a singular configuration. This can be found by studying the degeneracy of the direct kinematic model. Thus, there are Type 2 singularities if the following holds.

1. $\mathcal{E}(C_3)$ is an ellipse tangent to $\mathcal{L}_3$: in such a case, the directions of the three forces R_i intersect at one point W and the robot gains one infinitesimal rotation about this point (Figure 6a).

2. $\mathcal{L}_1$, $\mathcal{L}_2$ and $\mathcal{L}_3$ are parallel and $\mathcal{E}(C_3)$ degenerates to two lines parallel to $\mathcal{L}_1$ and $\mathcal{L}_2$ (and $\mathcal{L}_3$): in such a case, the directions of the three forces R_i are parallel and the robot gains one self-motion of translation (Figure 6b).

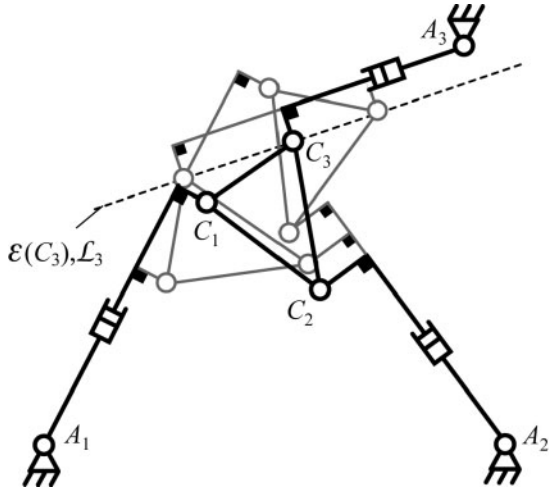

Fig. 7. Cardanic self-motion.

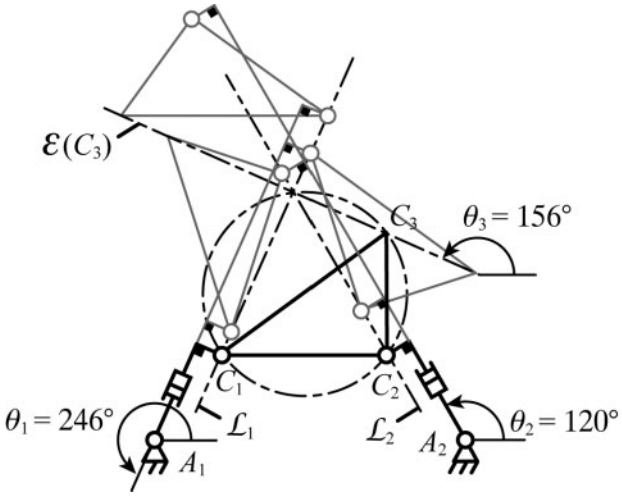

Fig. 8. Example of Cardanic motion for a 3-$\underline{R}PR$ planar parallel robot with $R_p = 0.2$ m, $R_b = 0.35$ m, $L_1 = L_2 = 0.05$ m (L_3 can be arbitrary), $\alpha_p = 36^\circ$ and $\beta_p = 72^\circ$.

3. $\mathcal{E}(C_3)$ degenerates to a doubly-traced line segment parallel to $\mathcal{L}_3$: this case will be discussed in detail in Section 3.

3. Analysis of Self-motions

Self-motions are certainly the worst type of singularity a parallel robot can encounter. If the robot enters such a singularity, since there are infinitely many possible poses for the same active-joint variables, the information on the pose of the platform is lost. For the robot under study, one could think that such singularities exist only when $\mathcal{L}_1$, $\mathcal{L}_2$ and $\mathcal{L}_3$ are parallel. In this case, we observe the apparition of a self-motion of translation, corresponding to the case shown in Figure 6b.

It turns out that a second, more complicated, case of self-motion appears when $\mathcal{E}(C_3)$ degenerates into a doubly-traced line segment parallel to $\mathcal{L}_3$. This case corresponds to a Cardanic self-motion (Figure 7). Note that such a singularity is a particular case of singular configuration where the three forces $\mathbf{R}_i$ intersect at one point W (Figure 6a).

3.1. Design Conditions Leading to Cardanic Self-motions

We have to find the geometric conditions that lead to Cardanic self-motions, i.e. when the ellipse $\mathcal{E}(C_3)$ degenerates into a doubly-traced line segment. This happens when y_{C3} is linearly dependent upon x_{C3} for $\sin(\theta_1 - \theta_2) \neq 0$. Rearranging Equation (13), we obtain:

$$\mathbf{OC}_3 = \begin{bmatrix} x_{C3} \\ y_{C3} \end{bmatrix} = \begin{bmatrix} b_{11} \\ b_{21} \end{bmatrix} + \mathbf{b} \begin{bmatrix} \cos\phi \\ \sin\phi \end{bmatrix}, \text{ where}$$

$$\mathbf{b} = \begin{bmatrix} b_{12} & b_{13} \\ b_{22} & b_{23} \end{bmatrix}. \tag{20}$$

$\mathcal{E}(C_3)$ will degenerate to a doubly-traced line if the determinant of matrix $\mathbf{b}$ vanishes. This would be the case if

$$\theta_1 = \theta_2 + \varepsilon_p, \quad \text{where} \quad \varepsilon_p = \alpha_p \pm \pi/2. \tag{21a}$$

As pointed out by one of the anonymous reviewers of this paper, this simple condition can also be directly obtained using the geometric properties of Cardanic motion. At each moment the intersection point between lines $\mathcal{L}_1$ and $\mathcal{L}_2$ lies on the circumcircle of the mobile platform.

For such a condition, it is therefore possible to find through algebraic manipulations that

$$y_{C3} = m(x_{C3} - b_{11}) + b_{21} \quad \text{and} \quad \theta_3 = \theta_2 + \delta_p \tag{21b}$$

where $m = \tan\theta_3$ and $\delta_p = \beta_p/2 + n\pi$ ($n = 0, 1, 2, \ldots$). Once again, this condition can also be obtained using the fact that at each moment the intersection point between lines $\mathcal{L}_2$ and $\mathcal{L}_3$ lies on the circumcircle of the mobile platform. It can also be shown that lines $\mathcal{L}_1$, $\mathcal{L}_2$ and $\mathcal{L}_3$ are concurrent.

Therefore, when $\mathcal{L}_1$ and $\mathcal{L}_2$ make an angle of ε_p and $\mathcal{L}_2$ and $\mathcal{L}_3$ make an angle of δ_p, the robot gains a Cardanic self-motion (Figure 8). However, at this stage, it is not clear whether any design allows self-motions or only particular (symmetric) ones.

Let us now find the conditions for the existence of Cardanic self-motions. Introducing conditions (21a) and (21b) into Equation (16), it turns out that terms c_2 and c_3 are equal to zero. The equation can therefore be simplified as:

$$c_1 = 0. \tag{22}$$

Developing Equation (22) and expressing c_1 as a function of the sine and cosine of θ_2, we obtain

$$c_1 = d_1 \cos\theta_2 + d_2 \sin\theta_2 + d_3 = 0, \tag{23}$$

where

$$d_1 = R_b\left(\sin(\delta_p + \alpha_b - \beta_b) - \sin(\alpha_b - \delta_p)\right), \quad (24)$$

$$\begin{aligned} d_2 = {} & R_b\left(\sin(\delta_p + \varepsilon_p + \alpha_b - \beta_b)\right. \\ & - \sin(\delta_p - \varepsilon_p + \alpha_b - \beta_b) - \sin(\varepsilon_p + \alpha_b - \delta_p)\big) / \sin\varepsilon_p \\ & - R_b\left(\sin(-\varepsilon_p + \alpha_b - \delta_p)\right. \\ & + 2\sin(-\varepsilon_p + \alpha_b + \delta_p)\big) / \sin\varepsilon_p, \end{aligned} \quad (25)$$

$$d_3 = \frac{L_1 \sin\delta_p - L_2 \sin(\delta_p - \varepsilon_p) - L_3 \sin\varepsilon_p}{\sin\varepsilon_p}. \quad (26)$$

Two cases for the cancellation of Equation (23) must therefore be examined:

1. when Equation (23) is satisfied only for some sets of active-joint angles;
2. when Equation (23) is satisfied for any θ_2, which is only possible if $d_1 = d_2 = d_3 = 0$.

Let us begin with the first case. The sets of active-joint variables satisfying Equation (23) can be found as:

$$\theta_{2p} = 2\tan^{-1}\left(\frac{-d_2 + \sqrt{d_2^2 + d_1^2 - d_3^2}}{d_3 - d_1}\right), \quad (27a)$$

$$\theta_{2m} = 2\tan^{-1}\left(\frac{-d_2 - \sqrt{d_2^2 + d_1^2 - d_3^2}}{d_3 - d_1}\right). \quad (27b)$$

As angles δ_p and ε_p are defined with $n\pi$ $(n = 0, 1, 2, \ldots)$, the maximal number of sets of active-joint variables is equal to eight, depending on the working modes. As pointed out by one of the anonymous reviewers, these solutions correspond to the intersection of six limaçons defined as the loci of the intersection points between lines $\mathcal{L}_1$, $\mathcal{L}_2$ and $\mathcal{L}_3$ (which are concurrent for a Cardanic self-motion) for varying angle θ_2. Thus, the robot can have Cardanic self-motions for a maximum of eight sets of (or infinitely many) active-joint angles.

Now, the most useful result is that there obviously exist designs without Cardanic self-motions. The condition for non-existence of Cardanic self-motions is simply the condition that prevents Equation (23) having real solutions, i.e.

$$d_3^2 > d_2^2 + d_1^2. \quad (28)$$

Considering the simple case where the base and platform are similar (or even equilateral) triangles and the offsets are equal i.e. $L = L_1 = L_2 = L_3$, and introducing these new parameters in Equation (28), it can be found that the condition of non-existence of Cardanic self-motions is

$$L \neq 0. \quad (29)$$

There therefore exist simple symmetric designs without Cardanic self-motions.

Now, we saw that Cardanic self-motions appear (or not) for only several active-joint sets. However, for a particular design of 3-*RPR* planar parallel robot with congruent equilateral base and platform triangles, if condition (21) is satisfied there exists an infinity of active-joint sets for which the robot gains a Cardanic self-motion (Chablat et al. 2006). Thus, there must be design conditions for the robot to have Cardanic self-motion for any value of angle θ_2.

The second possibility for canceling Equation (23) consists of the cancellation of terms d_i of Equations (24–26). Resolving these three equations leads to

$$L_1 \sin\delta_p - L_2 \sin(\delta_p - \varepsilon_p) - L_3 \sin\varepsilon_p = 0 \quad (30)$$

and

$$\alpha_b = \alpha_p \quad \text{and} \quad \beta_b = \beta_p. \quad (31)$$

Thus, the base and the mobile platform should be similar triangles and condition (30) on the offsets must hold. Such conditions for Cardanic self-motions do not depend on the value of angle θ_2, as previously demonstrated in Chablat et al. (2006).

In summary, Cardanic self-motions can be avoided by constraining the design parameters of the 3-*RPR* planar parallel robot (Equation (28)). In the worst case, if the base and the mobile platform are similar and if $L_1 \sin\delta_p - L_2 \sin(\delta_p - \varepsilon_p) - L_3 \sin\varepsilon_p = 0$, there are Cardanic self-motions for infinitely many active-joint sets. Finally, if one wants to have similar or even equilateral base and platform triangles, one way of completely avoiding self-motions is to use equal non-zero offsets.

3.2. Kinematic Analysis of the Cardanic Self-motion

Let us now analyze the allowable displacement of the center P of the platform when the base and the mobile platform are similar triangles, i.e.

$$\theta_1 = \theta_2 + \varepsilon_p, \quad \theta_3 = \theta_2 + \delta_p,$$
$$L_1 \sin\delta_p - L_2 \sin(\delta_p - \varepsilon_p) - L_3 \sin\varepsilon_p = 0.$$

The expressions of the coordinates of point *P,* a function of θ_2, are found using the closure equation:

$$\mathbf{OP} = \mathbf{OA}_2 + \mathbf{A}_2\mathbf{B}_2 + \mathbf{B}_2\mathbf{C}_2 + \mathbf{C}_2\mathbf{P}. \quad (32)$$

Developing this expression, one can obtain:

$$\begin{aligned} \mathbf{OP} = \begin{bmatrix} x \\ y \end{bmatrix} = \begin{bmatrix} x_{A2} \\ y_{A2} \end{bmatrix} + \rho_2 \begin{bmatrix} \cos\theta_2 \\ \sin\theta_2 \end{bmatrix} \\ + L_2 \begin{bmatrix} -\sin\theta_2 \\ \cos\theta_2 \end{bmatrix} - R_p \begin{bmatrix} \cos(-\alpha_p + \phi) \\ \sin(-\alpha_p + \phi) \end{bmatrix}, \end{aligned} \quad (33)$$

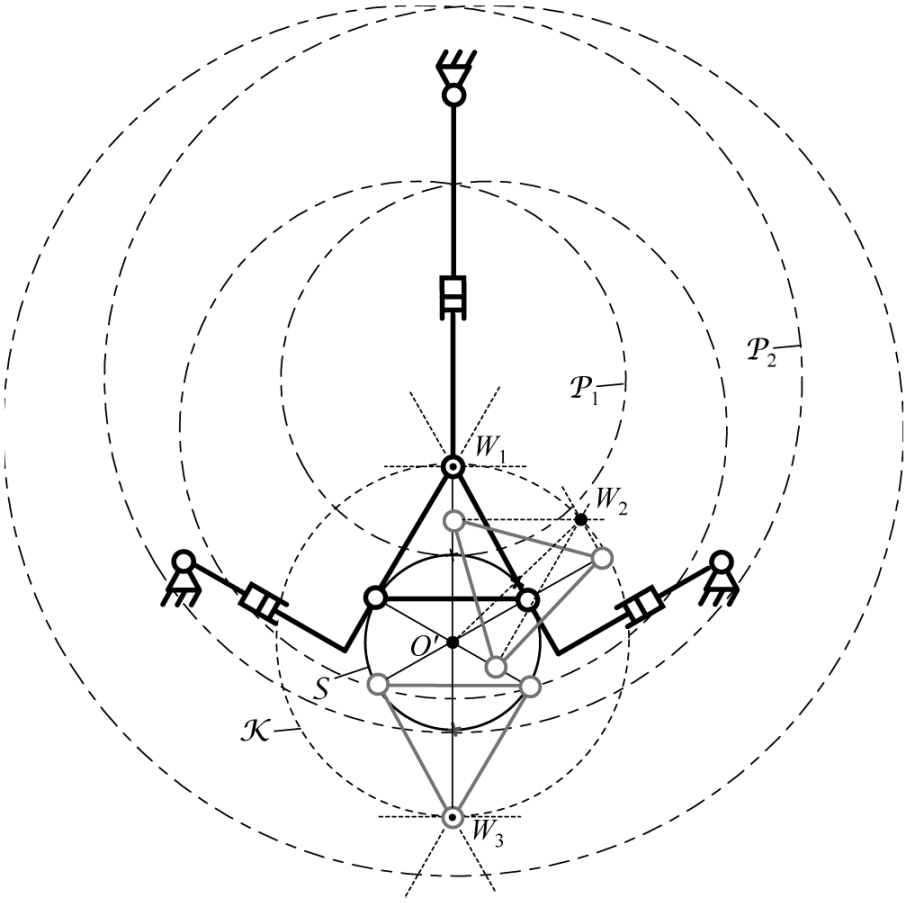

Fig. 9. Schematics of a Cardanic self-motion of a robot with $R_p = 0.1$ m, $R_b = 0.35$ m, $L_1 = L_2 = 0.07$ m, $L_3 = 0$ m, $\alpha_b = 30^\circ$ and $\beta_b = 120^\circ$.

where the expression of ρ_2 is given by Equation (12). Developing and introducing Equations (21), (30) and (31) in (33), it can be found that

$$\mathbf{OP} = \begin{bmatrix} R_p \cos(\alpha_p + 2\theta_2 - \phi) \\ -R_b \cos(\alpha_p + 2\theta_2) \\ -L_2 \sin(\theta_2 + \alpha_p) - L_1 \cos\theta_2 \\ R_p \sin(\alpha_p + 2\theta_2 - \phi) \\ -R_b \sin(\alpha_p + 2\theta_2) \\ +L_2 \cos(\theta_2 + \alpha_p) - L_1 \sin\theta_2 \end{bmatrix}. \quad (34)$$

From the previous expression it is possible to conclude that by varying the orientation ϕ of the mobile platform, point P moves in a circle $\mathcal{S}$ centered at O' whose radius is R_p (Figure 9). The coordinates of point O' are defined:

$$\mathbf{OO'} = -R_b \begin{bmatrix} \cos(\alpha_p + 2\theta_2) \\ \sin(\alpha_p + 2\theta_2) \end{bmatrix} + L_2 \begin{bmatrix} -\sin(\theta_2 + \alpha_p) \\ \cos(\theta_2 + \alpha_p) \end{bmatrix} - L_1 \begin{bmatrix} \cos\theta_2 \\ \sin\theta_2 \end{bmatrix}. \quad (35)$$

Computing the expressions of the coordinates of point W, the intersection point of the three wrenches $\mathbf{R}_i$, one obtains:

$$\mathbf{OW} = \begin{bmatrix} 2R_p \cos(\alpha_p + 2\theta_2 - \phi) \\ -R_b \cos(\alpha_p + 2\theta_2) \\ -L_2 \sin(\theta_2 + \alpha_p) - L_1 \cos\theta_2 \\ 2R_p \sin(\alpha_p + 2\theta_2 - \phi) \\ -R_b \sin(\alpha_p + 2\theta_2) \\ +L_2 \cos(\theta_2 + \alpha_p) - L_1 \sin\theta_2 \end{bmatrix}. \quad (36)$$

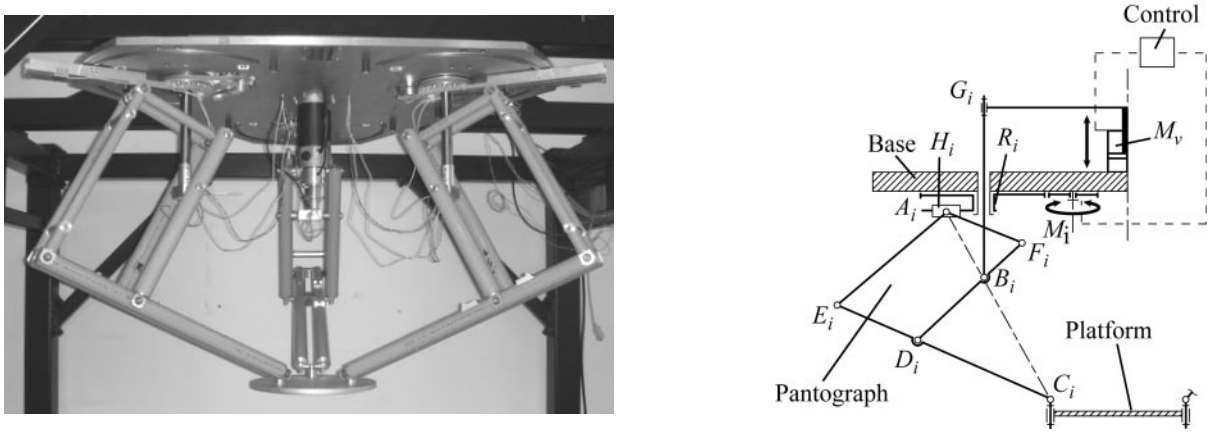

Fig. 10. The PAMINSA parallel robot: (a) prototype of the PAMINSA robot and (b) kinematic chain.

Thus, W is located on a circle $\mathcal{K}$ centered at O' whose radius is $2R_p$. It is also possible to observe that the platform and vector **O'P** rotate in opposite senses.

One can rearrange Equation (34) as follows:

$$\mathbf{OP} = \begin{bmatrix} R\cos(\eta + 2\theta_2) - L_2\sin(\theta_2 + \alpha_p) \\ -L_1\cos\theta_2 \\ R\sin(\eta + 2\theta_2) + L_2\cos(\theta_2 + \alpha_p) \\ -L_1\sin\theta_2 \end{bmatrix} \tag{37}$$

with

$$R = \sqrt{R_b^2 + R_p^2 - 2R_bR_p\cos\phi} \quad \text{and}$$

$$\eta = \tan^{-1}\left(-\frac{R_p\sin(\phi - \alpha_p) - R_b\sin\alpha_p}{R_p\cos(\phi - \alpha_p) - R_b\cos\alpha_p}\right). \tag{38}$$

For a given angle ϕ and active-joint angle θ_2, Equation (37) represents the singularity loci (for the Cardanic self-motions only) of the robot with specified parameters. The obtained result corresponds to the parametric expression of an epicycloid $\mathcal{P}$. The epicycloids $\mathcal{P}_1$ and $\mathcal{P}_2$ represented in Figure 9 are the curves corresponding to angles $\phi = 0$ and $\phi = \pi$, respectively.

4. Example and Experimental Validations

A prototype of a new decoupled 4-DOF parallel robot called PAMINSA (Parallel Robot of the INSA, Figure 10) was developed in INSA de Rennes (Briot and Arakelian 2007). Such a robot with Schoenflies motions allows the decoupling of the displacements in a horizontal plane (two translations along the $\boldsymbol{x}$ and $\boldsymbol{y}$ axes and one rotation about axes parallel to $\boldsymbol{z}$) from the translation along a vertical axis (for details, see Briot and Arakelian 2007). This decoupling therefore allows the separation of the control laws between two different models:

1. a model for the horizontal displacements equivalent to the control model of the 3-*RPR* planar parallel robot (Figure 11a); and2.
2. a linear model for the vertical translation due to the use of the pantograph linkage (Figure 11b).

Thus, PAMINSA presents the same Type 2 singularities as a symmetric 3-*RPR* planar parallel robot, which will be studied in this section. Indeed, the planar projection of the prototype of the PAMINSA robot corresponds to a 3-*RPR* planar parallel robot whose base and platform are non-identical equilateral triangles and whose offsets are zero, $L_i = 0$. These conditions correspond to a robot with infinitely many Cardanic self-motions within its workspace.

Introducing these constraints into matrix **A** of Equation (3), we can find the determinant of this matrix as

$$\begin{aligned} D &= \frac{2R_p\cos\alpha_p(\sin(\alpha_p - \beta_p) - \sin\alpha_p)}{\rho_1\rho_2\rho_3} \\ &\times (R_b\cos\phi - R_p)(x^2 + y^2 \\ &- (R_b^2 + R_p^2 - 2R_pR_b\cos\phi)). \end{aligned} \tag{39}$$

Type 2 singularity loci for the PAMINSA occur when the above expression vanishes (Briot and Arakelian 2007). Thus, the robot is in a Type 2 singularity when:

$$\rho_i = \pm\infty, \quad \text{for} \quad i = 1, 2 \text{ or } 3 \tag{40}$$

or

$$\phi = \phi_s = \pm\cos^{-1}(R_p/R_b) \tag{41}$$

or

$$x^2 + y^2 = R_b^2 + R_p^2 - 2R_bR_p\cos\phi. \tag{42}$$

Condition (40) implies that the platform is located at an infinite distance from the center of the base frame. This is

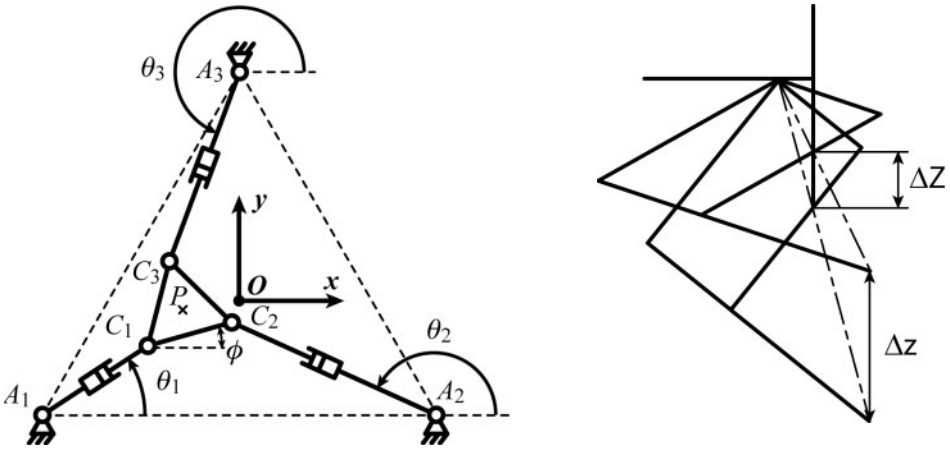

Fig. 11. The control models for the PAMINSA parallel robot: (a) model for the planar displacements and (b) model for the vertical translations.

equivalent to the fact that the three legs of the robot are parallel (Figure 6b). Condition (41) implies that the robot gains one degree of freedom for any position (x, y) of the workspace, for a fixed platform angle ϕ_s. Finally, condition (42) implies that the robot gains one degree of freedom when point P is located on a circle centered at O whose radius is $R = \sqrt{R_b^2 + R_p^2 - 2R_bR_p\cos\phi}$. Thus, we have to find which of the last two conditions correspond to Cardanic self-motions.

Introducing the constraints $L_i = 0$, $\alpha_b = \alpha_p$ and $\beta_b = \beta_p$ into Equation (34), we find

$$\mathbf{OP} = \begin{bmatrix} x \\ y \end{bmatrix} = \begin{bmatrix} R_p\cos(\alpha_p + 2\theta_2 - \phi) - R_b\cos(\alpha_p + 2\theta_2) \\ R_p\sin(\alpha_p + 2\theta_2 - \phi) - R_b\sin(\alpha_p + 2\theta_2) \end{bmatrix}. \quad (43)$$

Raising the norm of vector **OP** to square, we obtain Equation (42). Thus, this particular design of 3$\underline{R}$PR planar parallel robot gains one Cardanic self-motion when the end effector is positioned on a circle $\mathcal{P}$ centered at O and with radius equal to $R = \sqrt{R_b^2 + R_p^2 - 2R_bR_p\cos\phi}$ (Figure 9). The circles $\mathcal{P}_1$ and $\mathcal{P}_2$ represented in Figure 12 are the circles P corresponding to angles $\phi = 0$ and $\phi = \pi$, respectively.

Note that, for the angle ϕ_s, the robot gains one infinitesimal degree of freedom at any position, except if point P is located on a circle centered at O whose radius is equal to $R_s = \sqrt{R_b^2 + R_p^2 - 2R_bR_p\cos\phi_s}$. Such a position still corresponds to a Cardanic self-motion. Moreover, for $R_p = R_b$, the angle ϕ_s corresponds to a self-motion of translation (Chablat et al. 2006). This means that when the platform center is located at the circle $\mathcal{P}_1$, the platform gains two self-motions at the same time.

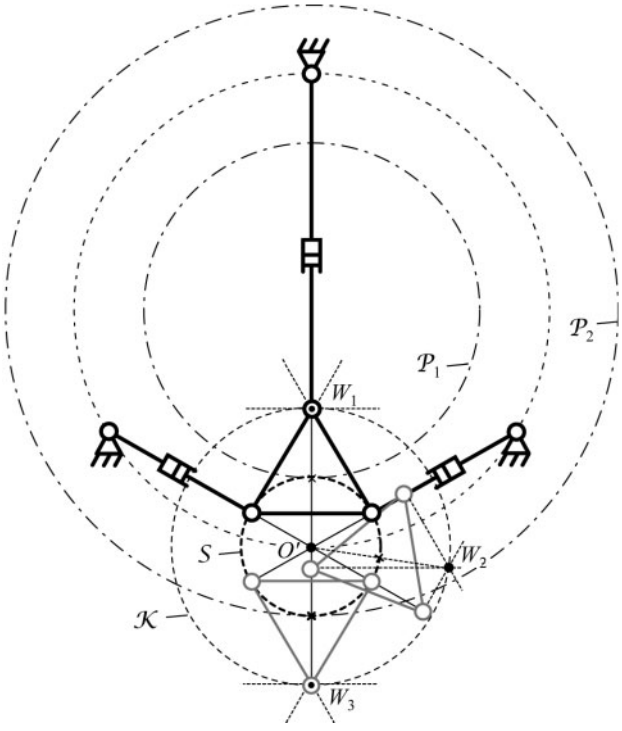

Fig. 12. Schematics of a Cardanic self-motion for a robot with $R_p = 0.1$ m, $R_b = 0.35$ m, $\alpha_b = 30^\circ$ and $\beta_b = 120^\circ$.

Observing Equation (43), it is possible to conclude that the degree of freedom gained is motion along a circle $\mathcal{S}$ centered at O' whose radius is R_p. The coordinates of point O' are:

$$\mathbf{OO'} = -R_b\begin{bmatrix} \cos(\alpha_p + 2\theta_2) \\ \sin(\alpha_p + 2\theta_2) \end{bmatrix}. \quad (44)$$

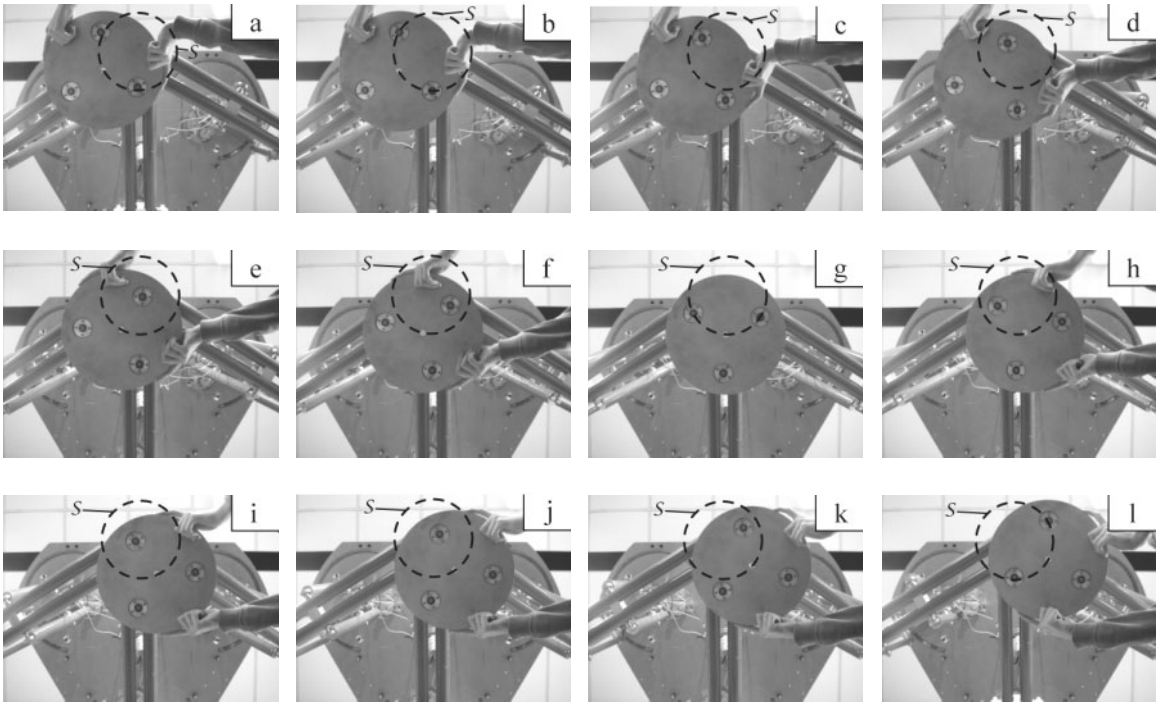

Fig. 13. Cardanic self-motion of the mobile platform of the PAMINSA prototype starting from the configuration x = 0 m, y = –0.25 m, $\phi = 0^\circ$.

Note that the circle $\mathcal{S}$ is tangent to circles $\mathcal{P}_1$ and $\mathcal{P}_2$. This means that the maximal singularity-free workspace is delimited by the circle $\mathcal{P}_1$. The radius of the circle $\mathcal{P}_1$ is equal to:

$$R_1 = \left| R_b - R_p \right| . \tag{45}$$

Dividing Equation (45) by R_b yields

$$\nu = R_1/R_b = \left| 1 - R_p/R_b \right| . \tag{46}$$

Therefore, the smaller the ratio R_p/R_b, the greater the value of ν. It is therefore possible to conclude that, for a larger singularity-free workspace, the rate R_p/R_b has to be smaller. However, the smaller the mobile platform with respect to the base, the less accurate is its orientation.

In order to demonstrate the previous results, we have positioned the PAMINSA prototype in a singular configuration with Cardanic self-motion (x = 0 m, y = -0.25 m, $\phi = 0^\circ$). This position is shown on Figure 13(g). For such a configuration, the three actuators are blocked. However, it is possible to see on Figures 13(a–e) that the platform is not constrained and undergoes a Cardanic self-motion when external force is applied to the platform.

5. Conclusions

In this paper, the singular configurations of general 3-*RPR* planar parallel robots were studied. It was shown that a general 3-*RPR* robot can have Cardanic self-motions for none, up to eight, or infinitely many active-joint sets. The conditions for having no self-motions or having self-motions for infinitely many active-joint sets were explicitly derived. It was shown, for example, that designs with similar (or even equilateral) base and platform triangles and equal offsets have no self-motions as long as the offsets are non-zero.

Acknowledgements

The authors thank the anonymous reviewers for their invaluable comments.

Appendix

Expressions for a_{ji} (j = 1, 2; i = 1, 2, 3):

$$a_{11} = \frac{(x_{A2} - x_{A1}) \sin\theta_2 + L_1 \cos(\theta_2 - \theta_1) - L_2}{\sin(\theta_2 - \theta_1)}$$

$$a_{12} = -\frac{2R_p \sin\theta_2 \cos\alpha_p}{\sin(\theta_2 - \theta_1)}$$

$$a_{13} = \frac{2R_p \cos\theta_2 \cos\alpha_p}{\sin(\theta_2 - \theta_1)}$$

$$a_{21} = \frac{(x_{A2} - x_{A1}) \sin\theta_1 - L_2 \cos(\theta_2 - \theta_1) + L_1}{\sin(\theta_2 - \theta_1)}$$

$$a_{22} = -\frac{2R_p \sin\theta_1 \cos\alpha_p}{\sin(\theta_2 - \theta_1)}$$

$$a_{23} = \frac{2R_p \cos\theta_1 \cos\alpha_p}{\sin(\theta_2 - \theta_1)}$$

Expressions for b_{ji} ($j = 1, 2$; $i = 1, 2, 3$):

$$b_{11} = x_{A1} + a_{11}\cos\theta_1 - L_1 \sin\theta_1$$

$$b_{12} = a_{12}\cos\theta_1 + 2R_p \cos\left(\alpha_p - \frac{\beta_p}{2}\right)\cos\frac{\beta_p}{2}$$

$$b_{13} = a_{13}\cos\theta_1 - 2R_p \cos\left(\alpha_p - \frac{\beta_p}{2}\right)\sin\frac{\beta_p}{2}$$

$$b_{21} = y_{A1} + a_{11}\sin\theta_1 + L_1 \cos\theta_1$$

$$b_{22} = a_{12}\sin\theta_1 + 2R_p \cos\left(\alpha_p - \frac{\beta_p}{2}\right)\sin\frac{\beta_p}{2}$$

$$b_{23} = a_{13}\sin\theta_1 + 2R_p \cos\left(\alpha_p - \frac{\beta_p}{2}\right)\cos\frac{\beta_p}{2}$$

Expressions of c_i ($i = 1, 2, 3$):

$$c_1 = (b_{21} - y_{A3})\cos\theta_3 + (x_{A3} - b_{11})\sin\theta_3 - L_3,$$

$$c_2 = b_{22}\cos\theta_3 - b_{12}\sin\theta_3, \quad c_3 = b_{23}\cos\theta_3 - b_{13}\sin\theta_3.$$

References

Bandyopadhyay, S. and Ghosal, A. (2004). Analysis of configuration space singularities of closed-loop mechanisms and parallel robots. *Mechanism and Machine Theory* **39**(5): 519–544.

Bonev, I.A., Zlatanov, D. and Gosselin, C.M. (2003). Singularity analysis of 3-DOF planar parallel mechanisms via screw theory. *Journal of Mechanical Design* **125**(3): 573–581.

Bonev, I.A., Chablat, D. and Wenger, P. (2006). Working and assembly modes of the Agile Eye. In *Proceedings of IEEE International Conference on Robotics and Automation*, Orlando, FL, USA, pp. 2317–2322.

Briot, S. and Arakelian, V. (2007). Singularity analysis of PAMINSA robot. In *Proceedings of 12th IFToMM World Congress*, Besançon, France.

Chablat, D., Wenger, P. and Bonev, I.A. (2006). Self-motions of a special 3-RPR planar parallel robot. *Advances in Robot Kinematics*, J. Lenarcic and B. Roth (eds.), Springer, pp. 221–228.

Gosselin, C.M. and Angeles, J. (1990). Singularity analysis of closed-loop kinematic chains. *IEEE Transactions on Robotics and Automation* **6**(3): 331–336.

Hayes, M.J.D. (1999). Kinematics of general planar Stewart-Gough platform. Ph.D. thesis. McGill University, Montreal, Quebec, Canada.

Hayes, M.J.D., Zsombor-Murray, P. and Chen, C. (2004). Unified kinematic analysis of general planar parallel robots. *Journal of Mechanical Design* **126**(5): 866–874.

Husty, M.L. and Zsombor-Murray, P. (1994). A special type of singular Stewart-Gough platform. *Advances in Robot Kinematics and Computational Geometry*, J. Lenarcic and B. Ravani (eds.), Kluwer Academic Publishers, pp. 449–458.

Husty, M.L. and Karger, A. (2000). Self-motions of Griffis-Duffy type parallel robots. In *Proceedings of IEEE International Conference on Robotic and Automation*, San Francisco, CA, USA, pp. 7–12.

Karger, A. (1998). Classification of 5R closed kinematic chain with self mobility. *Mechanism and Machine Theory* **33**(1): 213–222.

Karger, A. (2001). Singularities and self-motions of equiform platforms. *Mechanism and Machine Theory* **36**(7): 801–815.

Karger, A. (2003). Architecture singular planar parallel robots. *Mechanism and Machine Theory* **38**: 1149–1164.

Karger, A. and Husty, M.L. (1998). Classification of all self-motions of the original Stewart-Gough platform. *Computer-Aided Design* **30**(3): 205–215.

Merlet, J.-P. (1996). Direct kinematics of planar parallel robots. In *Proceedings of IEEE International Conference on Robotics and Automation*, Minneapolis, Minnesota, USA, pp. 3744–3749.

Sekulie, A. (1998). Method of synthesis of Cardanic motion. *Facta Universitatis*, Mechanical Engineering, University of NIS, **1**(5): 565–572.

Tischler, C.R., Hunt, K.H. and Samuel, A.E. (1998). A spatial extension of Cardanic movement: its geometry and some derived mechanisms. *Mechanism and Machine Theory* **33**(8): 1249–1276.

Wenger, P. and Chablat, D. (1998). Workspace and assembly modes in fully-parallel robots: a descriptive study. *Advances in Robot Kinematics and Computational Geometry*, Kluwer Academic Publishers, pp. 117–126.

Wohlhart, K. (2003). Mobile 6-SPS parallel robots. *Journal of Robotic Systems* **20**(8): 509–516.

Zlatanov, D., Fenton R.G. and Benhabib B. (1994). Singularity analysis of mechanisms and robots via a velocity-equation model of the instantaneous kinematics. In *Proceedings of IEEE International Conference on Robotics and Automation*, San Diego, CA, USA, pp. 980–991.